Editors' Suggestion

Magnetoelectric coupling in the multiferroic hybrid-improper ferroelectric $Ca_3Mn_{1.9}Ti_{0.1}O_7$

Yannik Zemp,[1] Morgan Trassin,[1] Elzbieta Gradauskaite,[1] Bin Gao,[2] Sang-Wook Cheong,[2] Thomas Lottermoser,[1] Manfred Fiebig,[1,*] and Mads C. Weber[1,3,†]

[1]*Department of Materials, ETH Zurich, 8093 Zurich, Switzerland*

[2]*Department of Physics and Astronomy and Rutgers Center for Emergent Materials, Rutgers University, New Brunswick, New Jersey 08901, USA*

[3]*Institut des Molécules et Matériaux du Mans, UMR 6283 CNRS, Le Mans Université, 72085 Le Mans, France*

(Received 19 November 2023; revised 4 March 2024; accepted 7 March 2024; published 8 May 2024)

Magnetic hybrid-improper ferroelectrics show potential for multiferroicity that is mediated by nonpolar structural distortions that give rise to both ferroelectricity and a net-magnetic spin canting. Here, we report on a pronounced magnetoelectric response of the ferroelectric state to the intrinsic magnetic ordering and to external magnetic fields in $Ca_3Mn_{1.9}Ti_{0.1}O_7$, a layered perovskite-type system. We observe a sixfold increase in the temperature-dependent response of the polarization-induced optical second-harmonic-generation (SHG) signal to the magnetic order that we explain as a magnetically triggered interlayer coupling of the polar order. Furthermore, an applied magnetic field up to 3 T along the direction of the net magnetization enhances the polarization-induced SHG signal by about 30%. We interpret this as magnetic-field-induced spin canting, which possibly affects the Mn-O bonds and hence the polarization. Optical SHG is of particular advantage to this study as it provides access to the electric polarization with spatial resolution of its domains, unobstructed by the leakage currents that impede contact-based measurements. Our investigations advance the understanding and potential of a highly promising new category of multiferroic materials for magnetoelectric cross control and functionalization.

DOI: 10.1103/PhysRevB.109.184417

I. INTRODUCTION

Multiferroic materials exhibit ferroelectric and magnetic orders simultaneously. A strong coupling between both orders may provide an avenue for enhanced data-processing technology, where stable magnetic bits can be written in a fast and energy-efficient way by voltage pulses. However, insufficient magnetoelectric coupling with low spontaneous polarization, magnetization, or operating temperatures have impeded the functionalization of multiferroics in a magnetoelectric device [1–5]. Overcoming these obstacles calls for developing materials with new coupling pathways between the ferroelectric and magnetic orders [6].

An approach that holds great promise is the use of structural distortions to interlink the polar and magnetic orders. This was exemplified on the family of hexagonal rare-earth manganites and in composite multiferroics where the multiferroic order is emulated by a combination of magnetostrictive and piezoelectric constituents [7–9]. More recently, hybrid-improper ferroelectrics have emerged as a promising new class of geometric ferroelectrics. In these, the joint action of two nonpolar distortive modes violates inversion symmetry and gives rise to ferroelectric order [10–14]. Such hybrid-improper ferroelectrics can also host magnetic ions that give rise to complementary magnetic order [13,15], thus creating a type of "geometric" multiferroic [8].

The prototypical example for these multiferroic hybrid-improper ferroelectrics is $Ca_3Mn_2O_7$. Its Mn^{4+} spins order antiferromagnetically in a G_x-type fashion [13,15]. Through Dzyaloshinskii-Moriya interaction (DMI), the tilting of the MnO_6 octahedra activates a ferromagnetic canting of the spins [15]. Hence, intriguingly, both the ferroelectric and the ferromagnetic orders are triggered by tilts of the MnO_6 octahedra. This suggests itself as a promising source for pronounced magnetoelectric coupling effects in this unique class of multiferroics [13]. A modulation of the magnetization by electric fields has indeed been shown experimentally [16,17]. Unfortunately high dielectric losses of these samples limit the applicable voltages and the response they triggered were small. Leakage currents are a general issue for voltage- and contact-based techniques in $Ca_3Mn_2O_7$ and related compounds [18]. Here the introduction of other techniques efficiently probing the magnetoelectric correlations would be helpful.

Using optical SHG as such a technique, we investigate the reverse magnetoelectric coupling, that is, the impact of the magnetic on the ferroelectric order, an aspect that has remained elusive so far. We report a sixfold increase in the temperature-dependent response of the polarization-related SHG signal as a result of the magnetic ordering of the hybrid-improper ferroelectric $Ca_3Mn_{1.9}Ti_{0.1}O_7$ (CMTO). We associate the magnetoelectric response with a magnetostrictive augmentation of interlayer coupling, which is instigated by the magnetic ordering and enhances the spontaneous polarization. We complement this passive form of magnetoelectric effect by active magnetoelectric control with an applied

*manfred.fiebig@mat.ethz.ch
†mads.weber@univ-lemans.fr

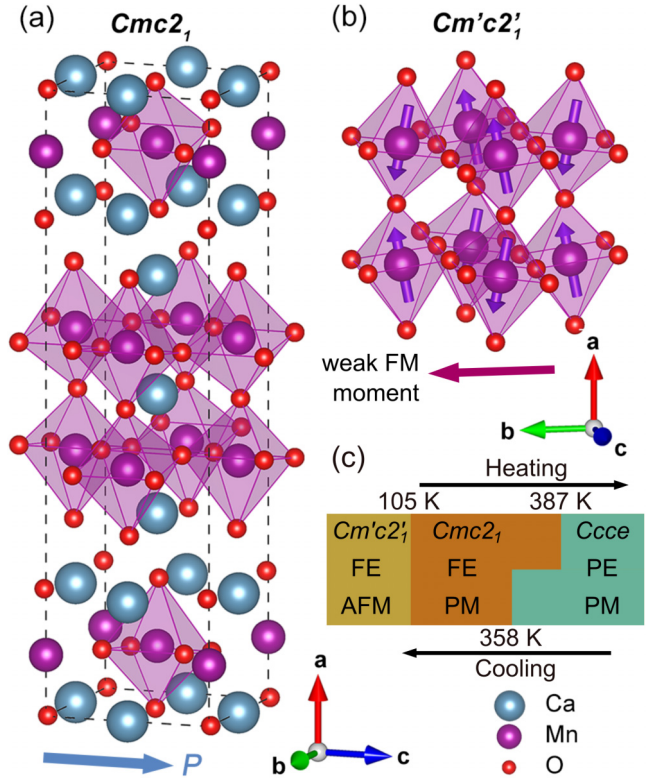

FIG. 1. (a) Orthorhombic room-temperature crystal structure of CMTO with the polar space group $Cmc2_1$. The ferroelectric polarization points along the c axis. (b) Magnetic structure below 105 K with the magnetic space group $Cm'c2'_1$, shown for a double-perovskite block. The magnetic order is of antiferromagnetic G_x type with additional weak ferromagnetic (F_y type) and antiferromagnetic cantings (C_z type) along the b and c directions, respectively. (c) Structural, electric, and magnetic phases encountered in heating and cooling runs [15,18–20]. The electric and magnetic properties of the different phases are given below their respective space groups as paraelectric (PE), ferroelectric (FE), paramagnetic (PM), and antiferromagnetic (AFM). The directions described by the indices (x, y, z) are parallel to the crystallographic axes (a, b, c). Structures are drawn using the software VESTA [21].

magnetic field. The field acts on the spin canting of the CMTO, which tunes the polarization-induced SHG signal within a 30% bracket. Optical SHG is of particular advantage to our investigation. It provides access to the electric polarization with spatial resolution of its domains, and it is not obstructed by the high dielectric losses that hamper contact-based measurements.

II. MULTIFERROIC ORDER OF $Ca_3Mn_{1.9}Ti_{0.1}O_7$

CMTO is isostructural to $Ca_3Mn_2O_7$, sharing qualitatively the same structural, polar, and magnetic properties. The Ti substitution enhances the crystal quality and slightly decreases the magnetic phase-transition temperature [18]. The Ruddlesden-Popper structure of the compound depicted in Fig. 1 consists of double-perovskite Ca(Mn, Ti)O_6 layers separated by CaO sheets, yielding the tetragonal prototype space-group $I4/mmm$ [15,19,22]. Below 1150 K, the material becomes orthorhombic with the space-group symmetry $Ccce$ [18,23]. When cooling, CMTO experiences a transition to the $Cmc2_1$ phase at 358 K. This phase is characterized by nonpolar tilt modes of the (Mn, Ti)O_6 octahedra of X_2^+ and X_3^- symmetry (X_2^+: $a^0a^0c^+$ and X_3^-: $a^-a^-c^0$ in the Glazer notation [24]). Remarkably, these nonpolar modes jointly break the inversion symmetry and activate a Γ_5 mode, a polar displacement of the Ca^{2+} cations along the orthorhombic c axis [13,19,22]. With this, CMTO becomes ferroelectric, a structure it retains down to cryogenic temperatures. For this type of ferroelectric state the term "hybrid improper" was coined. The magnitude of its spontaneous polarization P_s is proportional to the amplitudes of the two octahedra tilts

$$P_s \propto Q_{X_2^+} Q_{X_3^-}. \tag{1}$$

Because of the resulting trilinear coupling in the free energy

$$F \propto P_s Q_{X_2^+} Q_{X_3^-}, \tag{2}$$

the polarization changes sign upon reversal of either type of rotation of the octahedra [11,13]. Importantly, the transition at 358 K allows for two ferroelastic domain states with parallel a axes and their local bc planes rotated by 90° with respect to each other.

At $T_N = 105$ K, the Mn^{4+} spins order in an antiferromagnetic (AFM) G_x-type fashion [Fig. 1(b)] described by the magnetic space group $Cm'c2'_1$. Dzyaloshinskii-Moriya-type spin-orbit interaction between the manganese spins and the surrounding tilted oxygen octahedra leads to a collective spin canting [15]. This results in a weak magnetic moment along the b axis (F type) and an additional weak antiferromagnetic component along the c axis (C type).

According to theory [13], inverting the X_3^- rotation of the octahedra changes both the weak magnetic moment and the polarization direction. Conversely, inverting the X_2^+ rotation of the octahedra should flip the polarization without affecting the magnetization. This indicates that the X_3^- mode acts as the mediator of the magnetoelectric coupling. A magnetic field reverses the magnetization and with it the antiferromagnetic order, but not the octahedra tilts or the polarization.

III. EXPERIMENTAL

CMTO single crystals were grown by the floating-zone method as detailed elsewhere [18]. The cleaved crystals exhibit planar regions perpendicular to the a axis and a ferroelastic multidomain configuration. To probe the ferroelectric state and spatially resolve the domain structure, we use optical SHG. This technique is highly sensitive to symmetry and symmetry breaking by long-range order. The leading electric-dipole-type order of the SHG process is only allowed in systems with broken inversion symmetry and therefore couples directly to the ferroelectric polarization via the second-order susceptibility $\hat{\chi}^{(2)} = \hat{\chi}_0^{(2)} \vec{P}_s$ [25]. Electric-dipole-type SHG is given by $P_i(2\omega) = \epsilon_0 \chi_{ijk}^{(2)} E_j(\omega) E_k(\omega)$. It links the polarization components of the incoming fundamental light $E_{j,k}(\omega)$ to the polarization component of the induced nonlinear polarization $P_i(2\omega)$, which acts as source of a frequency-doubled light wave emitted from the SHG-active material. The nonzero components of $\hat{\chi}^{(2)}$ are defined by the point-group symmetry of the system. The explicit set of $\chi_{ijk}^{(2)}$

tensor components for CMTO is given in the Supplemental Material [26].

Because of the opacity of the CMTO samples, we performed SHG reflection experiments, using a Coherent Elite Duo Ti:sapphire laser amplifier system (central wavelength 800 nm (∼1.55 eV), pulse length ∼125 fs, repetition rate 1 kHz). The laser pumps an optical parametric amplifier (Coherent OPerA Solo), which, supplemented by frequency-mixing stages, allows to generate laser radiation between 3020 nm and 250 nm (0.41 and 4.96 eV, respectively). The incoming light was directed in near-normal incidence onto one ferroelastic domain of the optically flat *bc* cleavage plane of the samples. The polarization of the incident fundamental light and the detected SHG signal was selected by a half-wave plate and a Glan-Taylor prism, respectively. After passing the sample, colored-glass short- and long-pass filters suppressed the fundamental light and higher harmonics, respectively. SHG spectra were measured with a GaAs photomultiplier tube (Hamamatsu RS943-02) flanged onto a monochromator (Horiba Triax 180). We normalized the SHG spectra to the spectrally flat SHG response of a silver mirror to correct for the spectral dependence of the laser intensity and the beam profile and optical elements in the light path. Alternatively, for SHG imaging and temperature-dependent measurements, we used a liquid-nitrogen-cooled CCD camera (Photometrics AT200) as a detector. Here, a band-pass interference filter reduced stray light, and a microscope objective (Mitutoyo, ×20 magnification, 1 μm resolution, 2 cm working distance) allowed for high spatial resolution.

For measurements at low temperature, the sample was cooled in a liquid-helium-operated microcryostat (Janis SVT500, 10–300 K). For measurements under applied magnetic field, this was replaced by a superconducting-magnet cryostat (Oxford Instruments, Spectromag, 1.8–300 K, ⩽ 10 T). Finally, magnetization measurements were performed using a superconducting quantum interference device (SQUID, Quantum Design MPMS3, 1.8–400 K, ⩽ 7 T). Note that macroscopic SQUID magnetometry probes a mixture of the ferroelastic domain states unlike the spatially selective SHG measurements. To express this averaging effect, we are referring to a magnetic field applied parallel to the *bc* cleavage plane [18].

IV. RESULTS AND DISCUSSION

A. Magnetic phase transition

The magnetic order of CMTO assigns this hybrid-improper ferroelectric material to the class of multiferroics. For identifying the magnetic phase transition, we perform temperature-dependent magnetometry measurements. Figure 2(a) shows the temperature dependence of the Mn^{4+}-related net magnetization. A steep increase in magnetization [Fig. 2(a)] and the opening up of a magnetic hysteresis loop [Fig. 2(b)] marks the magnetic ordering temperature of 105 K, which is in excellent agreement with literature values [15,18]. The hysteresis loop broadens toward lower temperature, and the coercive field increases from 25 mT at 90 K to a maximum of 65 mT at 10 K.

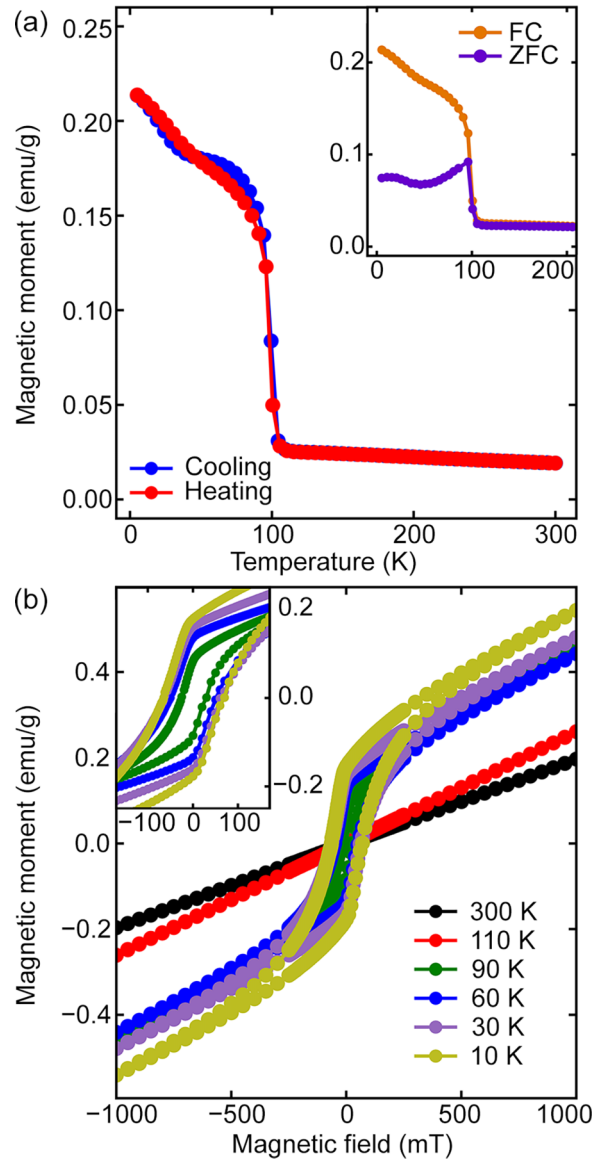

FIG. 2. (a) Magnetic moment of CMTO as a function of temperature for cooling and successive heating under an applied magnetic field of 100 mT in the *bc* plane. The magnetic phase transition is observed as a jump in the magnetic moment at around 105 K. Inset: Magnetic moment as a function of temperature for a zero-field-cooled and a field-cooled sample. (b) Magnetic hysteresis loops at different temperatures. Inset: Close-up of the low-field region. The remanent magnetic moment increases for lower temperatures. All magnetic fields were applied in the *bc* plane.

B. Evolution of the SHG signal across the magnetic phase transition

To investigate the ferroelectric response of CMTO to the magnetic ordering, we turn to SHG measurements. Here we make use of the relation $\hat{\chi}^{(2)} = \hat{\chi}_0^{(2)}\vec{P}_s$ from Sec. III. Figure 3 shows the spatially integrated, normalized SHG signal $I \propto |\vec{P}(2\omega)|^2$ of CMTO for heating and cooling runs at zero fields. At room temperature, the SHG signal associated with $\chi^{(2)}_{zzz}$ originates exclusively from the inversion-symmetry-breaking ferroelectric order emerging at $T_C = 358$ K [20]. Upon

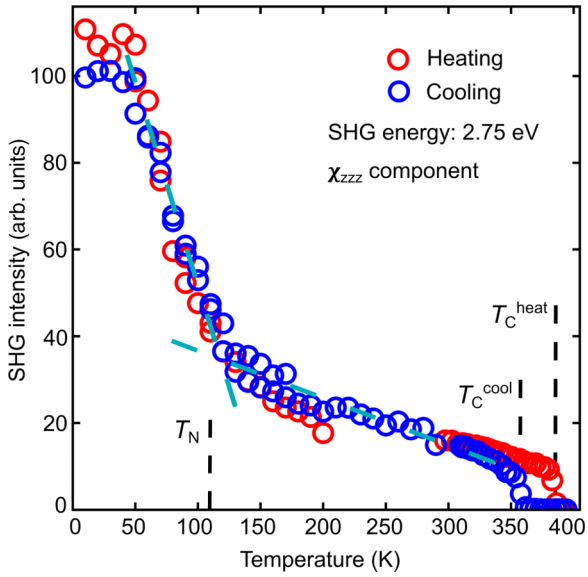

FIG. 3. SHG signal of the spontaneous-polarization-sensitive $\chi^{(2)}_{zzz}$ component as a function of temperature in successive heating and cooling runs, normalized to the extrapolated value at 0 K. The signal increases at a rate of 0.15 K^{-1} down to the magnetic phase-transition temperature. There, this slope increases by a striking factor of six until the SHG intensity saturates at ∼40 K. Green dashed lines are guides to the eye. Data between room temperature and 400 K adapted from [20].

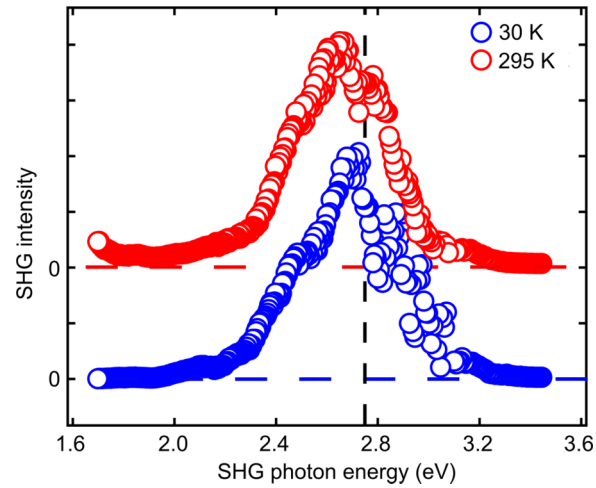

FIG. 4. Normalized SHG spectra of the $\chi^{(2)}_{zzz}$ component above and below the magnetic phase-transition temperature. The curves are normalized to their maximum values and vertically shifted for clarity. Vertical dashed line indicates 2.75 eV photon energy that was used for the SHG experiments.

cooling, the SHG intensity increases at a rate of 0.15 K^{-1} down to $T_N = 105$ K. With the onset of the magnetic order, a striking sixfold enhancement of this rate occurs before the SHG intensity saturates at 40 K. The data of the subsequent heating run overlap with the cooling curve, so hysteretic behavior is not observed.

Before we discuss the temperature dependence of the data in Fig. 3, we have to clarify the origin of the SHG signal. Its emergence at the ferroelectric Curie temperature associates the signal between T_N and T_C with the spontaneous polarization and, hence, with the magnitude of the octahedra tilts expressed by the X_2^+ and X_3^- modes because of $I \propto |\vec{P}(2\omega)|^2$ (see above) [20]. The temperature dependence can be attributed to the X_3^- octahedron tilt magnitude, which increases toward lower temperature, while the X_2^+ modes remains approximately constant [22]. The remarkable enhancement of the SHG signal below T_N can have different reasons that we discuss one by one in the following. We may have

(i) A change of the SHG spectrum.
(ii) SHG contributions from the magnetic order.
(iii) A shift in the ferroelectric domain population.
(iv) An increase of the spontaneous polarization.

(i) Figure 4 shows the normalized spectral dependence of the $\chi^{(2)}_{zzz}$-related SHG signal of ferroelectric CMTO above and below the magnetic-ordering temperature. We see that the spectral dependence changes only marginally between the two data sets. Hence, spectral shifts with temperature do not distort our SHG signal, which accounts for the photon energy of 2.75 eV used in all our experiments.

(ii) For the magnetic space-group symmetry $Cm'c2'_1$ of CMTO, the ferroelectric and the magnetic SHG contributions have the same set of nonzero SHG components $\chi^{(2)}_{ijk}$. Therefore, an identification of a magnetic SHG contribution via polarization-dependent SHG measurements is not possible. SHG contributions from the magnetic order would interfere with SHG contributions from the ferroelectric order, however. This interference would be constructive or destructive, depending on the magnetic and electric domain states that are combined, and thus lead to a sharp change in SHG brightness. We do not observe the emergence of such a contrast when we cool our samples below T_N, and this does not change when we apply a magnetic field below T_N that acts on the distribution of the magnetic domains. These two cases are depicted in Figs. 5 and 6, respectively. Figure 5(a) reveals the distribution of ferroelectric domains above T_N. Domains of opposite polarization do not exhibit a difference in brightness because of $I \propto |\vec{P}(2\omega)|^2$ with $P(2\omega) \propto \pm P_s$, see above. Destructive interference occurs at the domain walls, however, so that these become visible as black grooves [20,25,27] that are indicated by black arrows in Fig. 5(a). Below T_N, the distribution and brightness of the domains in Fig. 5(b) remain unchanged, which points to the absence of magnetization-related SHG contributions. Figure 6 shows the dependence of the SHG signal below T_N for a cycling magnetic field in the ±0.3-T range along the b axis. According to Fig. 2, the magnitude of our applied fields (±0.3 T) exceeds the measured coercive field of the weak magnetiztation of CMTO by over six times. Therefore, the here-applied fields transfer the region of interest between opposite magnetic single-domain configurations despite a possible slight shift in the coercive field due to the ferroelastic multidomain state probed by SQUID magnetometry in Fig. 2. Cycling magnetic field of ±0.3 T has no effect on the SHG yield and therefore supports the assumption that SHG contributions by the magnetic order are not detected. Both above and below T_N the SHG signal emitted by CMTO is of purely ferroelectric origin.

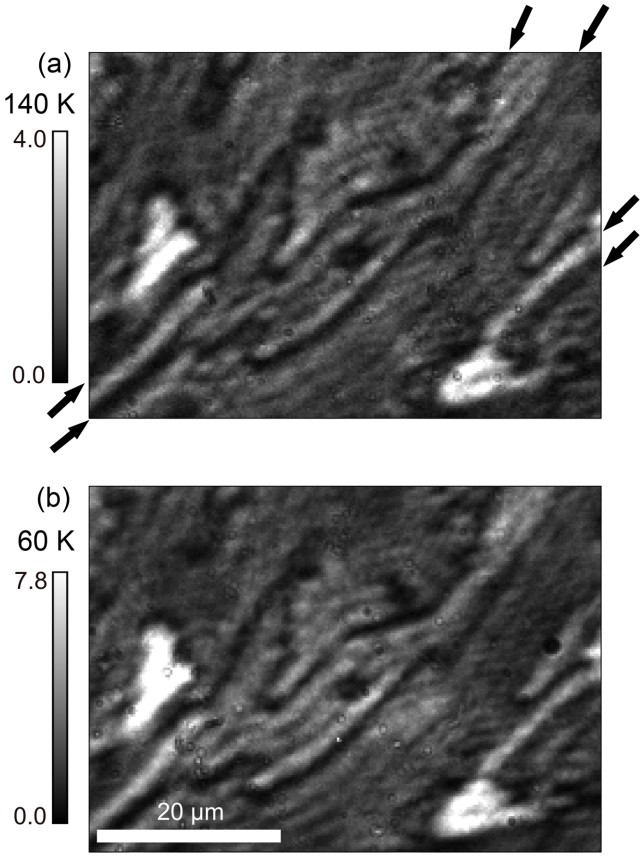

FIG. 5. (a), (b) Spatially resolved distribution of the SHG intensity on a CMTO sample above and below the magnetic phase transition at 105 K, respectively. Arrows indicate the position of selected ferroelectric domain walls, which are visible as black grooves because of an interference effect [20,25,27]. Bright patches are the result of interference between SHG contributions from opposite ferroelectric domains stacked perpendicular to the sample surface [20,27,28]. Image brightness is normalized to the respective mean values of the images.

(iii) The destructive interference of SHG contributions mentioned in point (iii) has an attenuating effect on the SHG yield of a spatially integrated measurement on a multidomain configuration. A shift in the ferroelectric domain population toward a single-domain configuration would diminish this attenuation and thus cause an increase of the SHG signal. Figure 5 reveals that the ferroelectric domain pattern above and below T_N is identical, however, so that we can exclude a shift in the ferroelectric domain population as origin of the SHG enhancement in Fig. 3.

(iv) The exclusion of options (i) to (iii) leaves an increase of the spontaneous polarization as only possible explanation for the steep increase of the SHG intensity below the magnetic ordering temperature. In the following, we discuss the origin of this remarkable magnetoelectric coupling in a multiferroic with hybrid-improper ferroelectricity. A simple attempt at an explanation would be to link the increase in P_s with an increase in the polarization-inducing tilts of the octahedra. In this interpretation, the drastic enhancement of P_s below T_N that follows from Fig. 3 would require an equally drastic increase in the tilt amplitudes of the octahedra. However, the

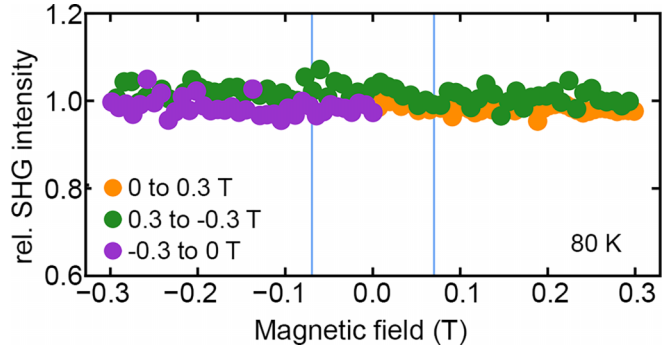

FIG. 6. Integrated SHG signal of the $\chi^{(2)}_{zzz}$ component in dependence of a magnetic field along the *b* axis after field cooling to 80 K. The blue vertical lines mark the coercive field of the weak magnetic moment, as extracted from Fig. 2(b).

structural distortion including increases of the tilt amplitudes induced by the magnetic ordering do not suffice to explain the enhancement of P_s [22,29–31].

Instead, we propose the emergence of a ferroelectric interlayer coupling by magnetically driven polar ordering of the (Mn, Ti)–O planes as the origin of the steep polarization enhancement below T_N. It was shown by Kong *et al.* for the hybrid-improper ferroelectric $(Ca, Sr)_3Ti_2O_7$ that the ferroelectric order evolves in two steps [32]. First, the polar order of the Ca–O planes emerges with the structural phase transition at T_C. It exhibits a weak interplane correlation and therefore behaves as quasi-two-dimensional. At lower temperature, polar order of the Ca–O planes is complemented by polar order of the Ti–O planes, which strengthens the interplane coupling and renders the ferroelectric order genuinely three-dimensional. This latter step enhances the spontaneous polarization of the $(Ca, Sr)_3Ti_2O_7$ system up to sixfold [32]. An equivalent evolution was reported for hybrid-improper ferroelectric $Li_2SrNb_2O_7$ [33]. In contrast, in CMTO the ferroelectric interlayer coupling of the (Mn, Ti)–O planes is stabilized by the Mn^{4+} spin order, as evidenced by the matching onsets of the magnetic order and the polarization enhancement in Fig. 3. The most likely explanation for the magnetoelectric stabilization of the interlayer coupling is a magnetostrictive distortion of the crystal structure including the Mn–O bond mediating the superexchange. We find evidence for this in the comparison of Refs. [32] and [22,29]. The latter works report an increase of the tilt of the octahedra with the onset of the magnetic order in CMTO and $Ca_3Mn_2O_7$, respectively. A corresponding increase is not found for the onset of the polar arrangement of the Ti–O planes in $Ca_3Ti_2O_7$, however. This shows that the magnetic order triggers the structural distortion through pronounced spin-lattice coupling [22,29–31], thus enhancing the spontaneous polarization as discussed. In turn, we can exclude the opposite dependence, where the onset of the ferroelectric interlayer coupling drives the magnetic order.

With CMTO, we thus have an interesting type of multiferroic of geometric origin where the polarization is impacted by the magnetic order. The structurally mediated magnetoelectric coupling changes the structural interlayer coupling and thus the magnitude of the ferroelectric polarization, yet not its

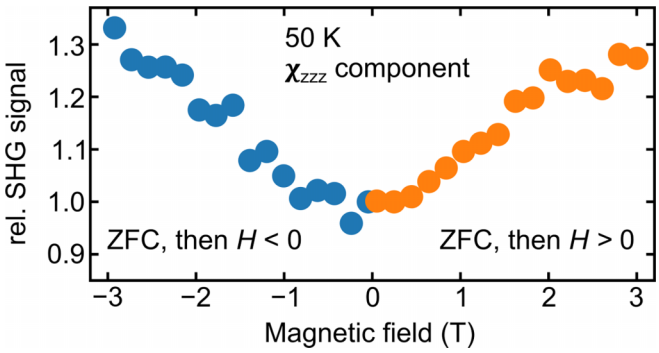

FIG. 7. Integrated SHG signal of the $\chi^{(2)}_{zzz}$ component in dependence of a magnetic field along the *b* axis after field cooling to 50 K. The SHG photon energy is 2.75 eV.

sign. On a macroscopic scale, the arrangement of ferroelectric domains remains therefore unaltered at all temperatures. This nuanced interaction between the magnetic and ferroelectric orders underscores the complexity of their interplay. More than just a direct relationship, it is a multifaceted interplay of distortive, electric, and magnetic elements.

C. Manipulation of the electric polarization

Now that we have understood the origin of the magnetoelectric coupling in multiferroic CMTO, we attempt to act on the ferroelectric order with an external magnetic field. For this, we apply a field along the *b* axis to exert a direct influence on the weak magnetization induced by DMI, which is oriented along *b*. Here we have to remember that the DMI describes a spin canting of superexchange-coupled ions in response to the tilt of the MnO_6 octahedra. In our experiment, we pursue the opposite path. The magnetic field enhances the canting of the Mn^{4+} spins and we investigate if this canting can act on the polarization, possibly by acting on the shift of the oxygen ions responsible for the superexchange of magnetic Mn^{4+} spins. As already discussed, a change in the Mn–O bond directly affects the polar order and, hence, the associated magnitude of the spontaneous polarization. Importantly, this excitation geometry prevents interfering contributions from the linear magnetoelectric effect and the magnetic-field-induced SHG because they are symmetry-forbidden for the measurement configuration chosen here (see Supplemental Material [26]). Any magnetic-field dependence of the SHG signal can then be attributed to the interaction between the applied magnetic field, the magnetic order, and the spontaneous electric polarization.

A magnetic field in the order of the coercive field acts on the distribution of the magnetization domains and can promote the region of interest toward a single-domain configuration. It does not change the magnetic order as such, however. Consistently, the application of magnetic fields up to 0.3 T in Fig. 6 does not cause a change of SHG intensity and, hence, of the associated spontaneous polarization. When higher magnetic fields are applied, the polarization-related SHG signal increases by up to 30% with only minor dependence on the sign of the magnetic field (Fig. 7). This shows that it is indeed possible to vary the spontaneous polarization P_s by an external magnetic field—presumptively through the inverse DMI as described above.

Note, for even higher magnetic fields and for field removal, the evolution of the SHG signal with the magnetic field becomes nontrivial and sample-history dependent, likely due to a spin reorientation as discussed in the Supplemental Material [26]. For the precise description of the magnetoelectric coupling mechanism under high magnetic fields, the exact knowledge of the magnetic order under high magnetic fields is required, which is beyond the scope of this work.

V. CONCLUSION

We have reported on magnetoelectric coupling effects in a new class of multiferroics, the magnetically ordered hybrid-improper ferroelectrics, here represented by CMTO. We observe a sixfold increase in the temperature-dependent response of polarization-related SHG signal with the onset of the magnetic order of the compound that we explain as magnetostrictively stabilized interlayer coupling of the polar order. We complemented this "passive" action of the magnetoelectric effect with "active" magnetoelectric polarization modification in a magnetic field. The field enhances the DMI-like ferromagnetism of the CMTO, which tunes the spontaneous polarization, possibly via the inverse DMI. With our experiments, we thus further open up one of the most promising new classes of multiferroic materials for magnetoelectric cross control and functionalization.

ACKNOWLEDGMENTS

The authors are grateful to Valerio Scagnoli and Saül Vélez for additional characterization measurements. This work was financially supported by SNSF (Grant No. 200021_178825/1) and European Research Council (Advanced Grant No. 694955-INSEETO). M.C.W. is grateful for financial support by the Région des Pays de la Loire under the Etoile Montante Initiative (Grant No. 2022_11808) and the PULSAR Academy. M.T. and E.G. acknowledge the financial support by the Swiss National Science Foundation under Project No. 200021_188414. The work at Rutgers University was supported by the DOE under Grant No. DOE: DE-FG02-07ER46382.

[1] N. A. Spaldin and R. Ramesh, Multiferroics: progress and prospects in thin films, Nat. Mater. **6**, 21 (2007).

[2] D. M. Evans, M. Alexe, A. Schilling, A. Kumar, D. Sanchez, N. Ortega, R. S. Katiyar, J. F. Scott, and J. M. Gregg, The Nature of magnetoelectric coupling in Pb(Zr, Ti)O_3-Pb(Fe, Ta)O_3, Adv. Mater. **27**, 6068 (2015).

[3] Y. Tokura and S. Seki, Multiferroics with spiral spin orders, Adv. Mater. **22**, 1554 (2010).

[4] Y. Tokunaga, Y. Taguchi, T.-H. Arima, and Y. Tokura, Electric-field-induced generation and reversal of ferromagnetic moment in ferrites, Nat. Phys. **8**, 838 (2012).

[5] E. Hassanpour, Y. Zemp, Y. Tokunaga, Y. Taguchi, Y. Tokura, T. Lottermoser, M. Fiebig, and M. C. Weber, Magnetoelectric transfer of a domain pattern, Science **377**, 1109 (2022).

[6] N. A. Spaldin and R. Ramesh, Advances in magnetoelectric multiferroics, Nat. Mater. **18**, 203 (2019).

[7] M. Giraldo, Q. N. Meier, A. Bortis, D. Nowak, N. A. Spaldin, M. Fiebig, M. C. Weber, and T. Lottermoser, Magnetoelectric coupling of domains, domain walls and vortices in a multiferroic with independent magnetic and electric order, Nat. Commun. **12**, 3093 (2021).

[8] M. Fiebig, *Nonlinear Optics on Ferroic Materials* (Wiley-VCH, Weinheim, 2023).

[9] C. W. Nan, M. I. Bichurin, S. Dong, D. Viehland, and G. Srinivasan, Multiferroic magnetoelectric composites: historical perspective, status, and future directions, J. Appl. Phys. **103**, 031101 (2008).

[10] N. A. Benedek, J. M. Rondinelli, H. Djani, P. Ghosez, and P. Lightfoot, Understanding ferroelectricity in layered perovskites: new ideas and insights from theory and experiments, Dalton Trans. **44**, 10543 (2015).

[11] A. T. Mulder, N. A. Benedek, J. M. Rondinelli, and C. J. Fennie, Turning ABO_3 antiferroelectrics into ferroelectrics: design rules for practical rotation-driven ferroelectricity in double perovskites and $A_3B_2O_7$ Ruddlesden-Popper compounds, Adv. Funct. Mater. **23**, 4810 (2013).

[12] Y. S. Oh, X. Luo, F.-T. Huang, Y. Wang, and S.-W. Cheong, Experimental demonstration of hybrid improper ferroelectricity and the presence of abundant charged walls in $(Ca, Sr)_3Ti_2O_7$ crystals, Nat. Mater. **14**, 407 (2015).

[13] N. A. Benedek and C. J. Fennie, Hybrid improper ferroelectricity: A mechanism for controllable polarization-magnetization coupling, Phys. Rev. Lett. **106**, 107204 (2011).

[14] N. A. Benedek, Origin of ferroelectricity in a family of polar oxides: the Dion-Jacobson phases, Inorg. Chem. **53**, 3769 (2014).

[15] M. V. Lobanov, M. Greenblatt, E. N. Caspi, J. D. Jorgensen, D. V. Sheptyakov, B. H. Toby, C. E. Botez, and P. W. Stephens, Crystal and magnetic structure of the $Ca_3Mn_2O_7$ Ruddlesden-Popper phase: neutron and synchrotron x-ray diffraction study, J. Phys.: Condens. Matter **16**, 5339 (2004).

[16] W. Zhu, L. Pi, Y. Huang, S. Tan, and Y. Zhang, Electrically induced decrease of magnetization in $Ca_3Mn_2O_7$, Appl. Phys. Lett. **101**, 192407 (2012).

[17] M. Liu, Y. Zhang, L.-F. Lin, L. Lin, S. Yang, X. Li, Y. Wang, S. Li, Z. Yan, X. Wang, X.-G. Li, S. Dong, and J.-M. Liu, Direct observation of ferroelectricity in $Ca_3Mn_2O_7$ and its prominent light absorption, Appl. Phys. Lett. **113**, 022902 (2018).

[18] B. Gao, F.-T. Huang, Y. Wang, J.-W. Kim, L. Wang, S.-J. Lim, and S.-W. Cheong, Interrelation between domain structures and polarization switching in hybrid improper ferroelectric $Ca_3(Mn, Ti)_2O_7$, Appl. Phys. Lett. **110**, 222906 (2017).

[19] M. S. Senn, A. Bombardi, C. A. Murray, C. Vecchini, A. Scherillo, X. Luo, and S. W. Cheong, Negative thermal expansion in hybrid improper ferroelectric Ruddlesden-Popper perovskites by symmetry trapping, Phys. Rev. Lett. **114**, 035701 (2015).

[20] M. C. Weber, Y. Zemp, M. Trassin, A. Simonov, J. Schaab, B. Gao, S.-W. Cheong, T. Lottermoser, and M. Fiebig, Asymmetric character of the ferroelectric phase transition and charged domain walls in a hybrid improper ferroelectric, Adv. Electron. Mater. **8**, 2100434 (2022).

[21] K. Momma and F. Izumi, *VESTA 3* for three-dimensional visualization of crystal, volumetric and morphology data, J. Appl. Crystallogr. **44**, 1272 (2011).

[22] F. Ye, J. Wang, J. Sheng, C. Hoffmann, T. Gu, H. J. Xiang, W. Tian, J. J. Molaison, A. M. Dos Santos, M. Matsuda, B. C. Chakoumakos, J. A. Fernandez-Baca, X. Tong, B. Gao, J. W. Kim, and S. W. Cheong, Soft antiphase tilt of oxygen octahedra in the hybrid improper multiferroic $Ca_3Mn_{1.9}Ti_{0.1}O_7$, Phys. Rev. B **97**, 041112(R) (2018).

[23] P. Rocha-Rodrigues, S. S. M. Santos, I. P. Miranda, G. N. P. Oliveira, J. G. Correia, A. L. V. C., H. M. Petrilli, J. P. Araújo, and A. M. L. Lopos, $Ca_3Mn_2O_7$ structural path unraveled by atomic-scale properties: A combined experimental and *ab initio* study, Phys. Rev. B **101**, 064103 (2020).

[24] A. M. Glazer, The classification of tilted octahedra in perovskites, Acta Cryst. B **28**, 3384 (1972).

[25] S. A. Denev, T. T. A. Lummen, E. Barnes, A. Kumar, and V. Gopalan, Probing ferroelectrics using optical second harmonic generation, J. Am. Ceram. Soc. **94**, 2699 (2011).

[26] See Supplemental Material at http://link.aps.org/supplemental/10.1103/PhysRevB.109.184417 for the tensors of the second harmonic generation process in CMTO, the magnetoelectric effect in CMTO, magnetic-field-induced SHG, and the magnetization of CMTO under high magnetic fields. The Supplemental Material also includes Refs. [34–37].

[27] M. Fiebig, D. Fröhlich, T. Lottermoser, and M. Maat, Probing of ferroelectric surface and bulk domains in $R\mathrm{MnO_3}$ (R=Y, Ho) by second harmonic generation, Phys. Rev. B **66**, 144102 (2002).

[28] B. B. Van Aken, J. P. Rivera, H. Schmid, and M. Fiebig, Anisotropy of antiferromagnetic 180° domains in $LiCoPO_4$ and $LiNiPO_4$, Phys. Rev. Lett. **101**, 157202 (2008).

[29] P. Sahlot, G. Sharma, V. Sathe, A. K. Sinha, and A. M. Awasthi, Interplay of spin, lattice, vibration, and charge degrees of freedom: Magneto-dielectricity in $Ca_3Mn_2O_7$, J. Am. Ceram. Soc. **103**, 3238 (2020).

[30] A. Glamazda, D. Wulferding, P. Lemmens, B. Gao, S. W. Cheong, and K. Y. Choi, Soft tilt and rotational modes in the hybrid improper ferroelectric $Ca_3Mn_2O_7$, Phys. Rev. B **97**, 094104 (2018).

[31] S. Liu, H. Zhang, S. Ghose, M. Balasubramanian, Z. Liu, S. G. Wang, Y.-S. Chen, B. Gao, J. Kim, S.-W. Cheong, and T. A. Tyson, Nature of the structural symmetries associated with hybrid improper ferroelectricity in $Ca_3X_2O_7$ (X = Mn and Ti), Phys. Rev. B **99**, 224105 (2019).

[32] J. Kong, A. Manjón-Sanz, J. Liu, F. Marlton, T. W. Lo, D. Lei, M. R. Vogel Jørgensen, and A. Pramanick, Scaling behavior of order parameters for the hybrid improper ferroelectric $(Ca, Sr)_3Ti_2O_7$, Phys. Rev. B **107**, 224103 (2023).

[33] R. Uppuluri, H. Akamatsu, A. Sen Gupta, H. Wang, C. M. Brown, K. E. Agueda Lopez, N. Alem, V. Gopalan, and T. E. Mallouk, Competing polar and antipolar structures in the Ruddlesden-Popper layered perovskite $Li_2SrNb_2O_7$, Chem. Mater. **31**, 4418 (2019).

[34] R. R. Birss, *Symmetry and Magnetism* (North-Holland Pub. Co., Amsterdam, 1966).

[35] M. Fiebig, Revival of the magnetoelectric effect, J. Phys. D **38**, R123 (2005).

[36] V. V. Pavlov, A. M. Kalashnikova, R. Pisarev, I. Sänger, D. R. Yakolev, and M. Bayer, Magnetic-field-induced second-harmonic generation in semiconductor GaAs, Phys. Rev. Lett. **94**, 157404 (2005).

[37] J. Blasco, J. A. Rodríguez-Velamazán, J. L. García-Muñoz, V. Cuartero, S. Lafuerza, and G. Subías, Structural and magnetic properties of $Ca_3Mn_{2-x}Ru_xO_7$ $(0 < x \leqslant 0.9)$, Phys. Rev. B **106**, 134403 (2022).